TEST OF QED AT CRITICAL FIELD STRENGTH

Christian Bula
Physics Department, Princeton University
Princeton, New Jersey 08544

Representing the E-144 Collaboration:
Princeton/Rochester/SLAC/Tennessee

ABSTRACT

In a new experiment at the Final Focus Test Beam at SLAC a low-emittance 46.6-GeV electron beam is brought into collision with terawatt pulses of 1054 nm or 527 nm wavelength from a Nd:glass laser. Peak laser intensities of 10^{18} W/cm^2 have been achieved corresponding to a value of 0.6 for the parameter $\eta = e\mathcal{E}/m\omega_0 c$. In this case an electron that crosses the center of the laser pulse has near-unit interaction probability. Results are presented for multiphoton Compton scattering in which an electron interacts with up to 4 laser photons, in agreement with theoretical calculations.

1 Introduction

The interaction of electrons with intense wave fields was first considered by Schott[1] which led to the introduction of the dimensionless measure of field strength

$$\eta = \frac{e\mathcal{E}_{\rm rms}}{m\omega_0 c} = \frac{e\mathcal{E}_{\rm rms}\lambda_0/2\pi}{mc^2} = \frac{e\sqrt{\langle A_\mu A^\mu \rangle}}{mc^2},$$

for a plane wave of laboratory frequency ω_0, wavelength λ_0, electric field E and four-vector potential A_μ. A field with $\eta = 1$ has a voltage drop of an electron rest mass per reduced laser wavelength $\lambda_0/2\pi$. In the average rest frame of an electron in a wave field the transverse motion has characteristic velocity $\beta^\star = v^\star/c$ related by $\gamma^\star\beta^\star = \eta$, where $\gamma = 1/\sqrt{1-\beta^2}$, so that parameter η is often called $v_{\rm osc}/c$ in weak fields. As η approaches and exceeds unity the classical radiation spectrum includes higher harmonics of the wave frequency ω_0 (multipole radiation). In the quantum view this corresponds to absorption of several wave photons before emission of a single photon of frequency ω:

$$e + n\omega_0 \to e' + \omega.$$

Only one observation of this effect has been reported: a weak signal of second-harmonic radiation in scattering of 1-keV electrons from a Q-switched Nd:YAG laser.[2] A closely related effect is higher-harmonic generation in a free-electron laser,[3] where η is often called k.

A quantum description of electrons in a strong wave field utilizes the Volkov solutions[4,5] to the Dirac equation, in which an electron is 'dressed' by continual absorption and re-emission of wave photons leading to an effective mass

$$\overline{m} = m\sqrt{1+\eta^2}.$$

The role of the effective mass in Compton scattering of electrons in a strong wave field was discussed by Sengupta[6] and others.[7–10] In nonuniform waves the effective energy $\overline{m}c^2$ is called the ponderomotive potential, which describes the forces on a charged particle as it enters or exits the wave.[11,12] Ponderomotive effects on electrons ejected from atoms in a wave field with $\eta \approx 1$ have recently been observed by Moore *et al.*.[13]

We report on an experiment in which 46.6-GeV electrons are scattered at the focus of an intense laser with wavelength $\lambda_0 = 1054$ (infrared) or 527 nm (green).

Under these conditions the photon energy in the rest frame of the electron beam is of order of the electron rest mass so that recoil effects are important. Absorption of a single photon corresponds to ordinary Compton scattering. However, at the laser intensities achieved ($I \approx 10^{18}$ W/cm^2, $\eta \approx 0.6$) the probability for multiphoton absorption is large and this effect was readily observed.

When n photons are absorbed by an electron of initial energy E_0 from a laser pulse with intensity parameter η and crossing angle θ_0 to the electron beam the minimum energy of the scattered electrons is

$$E_{\min} = E_0/[1 + 2nE_0\omega_0(1+\cos\theta_0)/\overline{m}^2].$$

The higher effective mass of the electron in the wave field shifts the minimum scattered energy to slightly higher values. For ordinary Compton scattering ($n = 1$) the minimum scattered-electron energy is 25.6 GeV at $E_0 = 46.6$ GeV, $\eta = 0$, and $\theta_0 = 17°$. The spectrum of electrons scattered by absorption of more than one laser photon extends below 25.6 GeV permitting an identification of multiphoton (nonlinear) Compton scattering.

Figure 1 shows spectra of scattered electrons calculated according to ref.[10] for conditions representative of the present experiment with $\eta = 0.5$. The calculation includes the space-time profiles of the electron and laser beams and makes the adiabatic approximation that the rate based on infinite plane waves holds for the local value of η. The calculation also includes the effect of multiple Compton scattering in which an electron undergoes successive ordinary Compton scatters at different points as it traverses the laser focus. This process is physically distinct from nonlinear Compton scattering in which several photons are absorbed at a single point and a single high-energy photon is emitted. Figure 2a represents $n = 2$ nonlinear Compton scattering, while Fig. 2b represents two successive ordinary Compton scatters. Electron e' in Fig. 2b is real. The black circles indicate that the absorption of a wave photon by an electron in a Volkov state is not simply described by a vertex factor of charge e.

The curves in Fig. 1 are labeled by the highest number of photons that are absorbed in a single scattering event. Thus the dashed curve labeled $n = 1$ corresponds to ordinary Compton scattering, but extends below 25.6 GeV because of multiple ordinary Compton scattering. The curve labeled $n = 2$ also extends below the nominal minimum energy for nonlinear Compton scattering because additional ordinary Compton scatters also occur. The upper solid curve is the sum

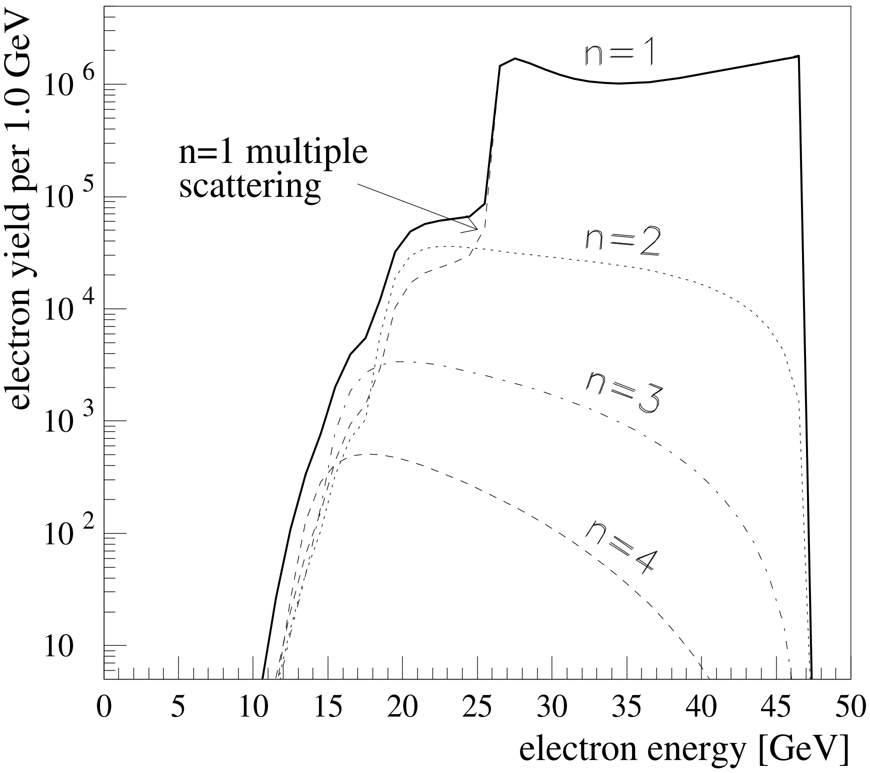

Figure 1: Calculated yield of scattered electrons from the collision of 5×10^9 46.6-GeV electrons with a circularly-polarized 1054-nm laser pulse with intensity parameter $\eta = 0.5$.

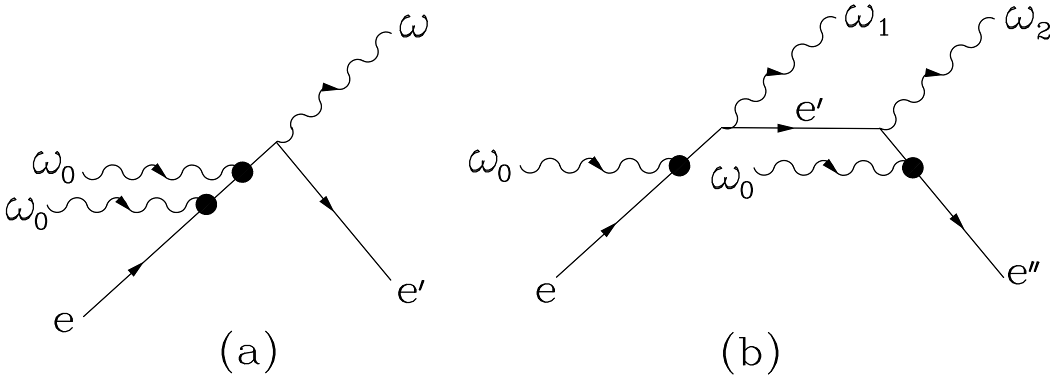

Figure 2: Diagrams representing (a) $n = 2$ nonlinear Compton scattering, and (b) double ordinary Compton scattering.

of all possible scatterings. Note that the simulated electron rates for $n = 2$ nonlinear Compton scattering and double ordinary Compton scattering are roughly equal in the energy range 20-25 GeV.

In quantum electrodynamics a natural measure of electromagnetic field strength is the so-called critical field for which the voltage drop across a Compton wavelength is an electron rest mass:

$$\mathcal{E}_{\rm crit} = \frac{m^2c^3}{e\hbar} = 1.3 \times 10^{16}\ \mathrm{V/cm} = 4.4 \times 10^{13}\ \mathrm{gauss}.$$

The critical field was first introduced by Sauter[14] as the characteristic field strength at which Klein's paradox[15] becomes important and was further interpreted by Heisenberg and Euler[16] as the field strength at which electron-positron pair creation becomes copious. For a particle in a strong wave field a useful dimensionless invariant is

$$\Upsilon = \frac{e\hbar}{m^3c^5}\sqrt{(F_{\mu\nu}p^\nu)^2} = \frac{\mathcal{E}^\star}{\mathcal{E}_{\rm crit}} \simeq \frac{2\gamma\mathcal{E}}{\mathcal{E}_{\rm crit}},$$

where $F_{\mu\nu}$ is the field tensor and p_ν is the particle's 4-vector; $\mathcal{E}^\star$ is the wave field in the particle's rest frame, and the final equality holds only if the particle is moving anticollinear to the wave with Lorentz boost γ. Static fields with values of Υ approaching one are thought to exist at the surface of neutron stars. The field at the surface of a nucleus has Υ less than one, but quasistatic fields with Υ exceeding unity arise in MeV heavy-ion collisions.

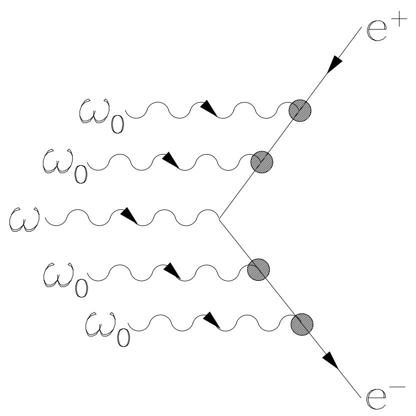

Figure 3: Diagram representing multiphoton pair creation.

Electron-positron creation can arise in the interactions of electrons with a wave in a two-step process in which a Compton-scattered photon collides with wave photons to produce the pair. Weak-field pair creation by photons was first considered by Breit and Wheeler,[17] and Reiss[18] first discussed the strong-field case,

$$\omega + n\omega_0 \to e^+e^-,$$

in which several wave photons participate; see also refs.[8,10] Figure 3 represents the latter process for a case where an external photon and four wave photons combine to produce a pair.

The present experiment studies the basic interactions of electrons and photons in fields near the QED critical field strength. It is also relevant to the understanding of so-called beamstrahlung processes at future e^+e^-colliders where the fields surrounding the beam bunches approach $\mathcal{E}_{\rm crit}$,[19] and where the consequent pair creation will be a limiting background. The experiment provides a demonstration of the technology for e-γ and γ-γ collider options,[20] leading to measurements of the γWW coupling via the reaction $e\gamma \to W\nu$,[21] *etc.* Copious production of positrons in e-γ collisions can provide a low-emittance positron source due to the absence of final-state Coulomb scattering.[22]

The parameters η and Υ are not independent, and for electrons colliding head-on with a wave their relation is $\Upsilon/\eta = 2\gamma\hbar\omega_0/mc^2$. For GeV electrons interacting with a laser the ratio of Υ to η is near one, so experiments in these conditions probe nonlinear effects due to both multiphoton absorption and vacuum polarization.

2 Experimental Setup

2.1 Phase I

The experiment presented here is carried out in the Final Focus Test Beam at SLAC.[23] The setup for the first phase of the experiment is shown schematically in Fig. 4. The laser is focused at the interaction point, IP1, 10 m downstream of the Final Focus. A set of permanent dump magnets is used to direct the electron beam downwards to the dump and also serves as the analyzing magnet of our experiment.

Compton-scattered electrons are deflected away from the primary electron beam by the dump magnets and are detected in a Silicon-Tungsten calorimeter (ECAL),[29] sketched in Fig. 5a. Positrons were deflected to the opposite side of

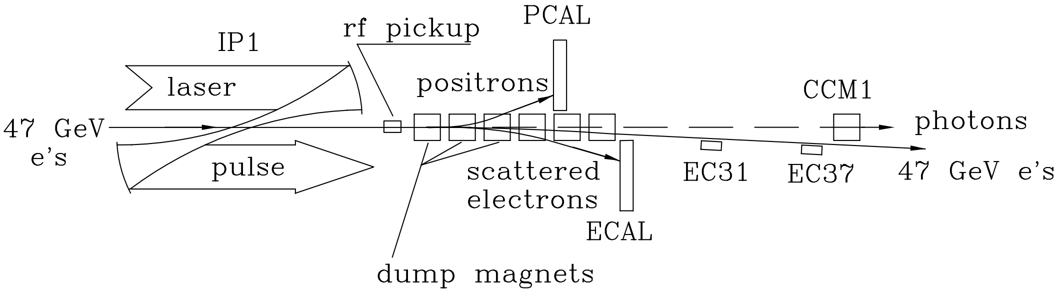

Figure 4: Sketch of experiment E-144 to detect scattered electrons and positrons produced in e-laser collisions at the SLAC Final Focus Test Beam.

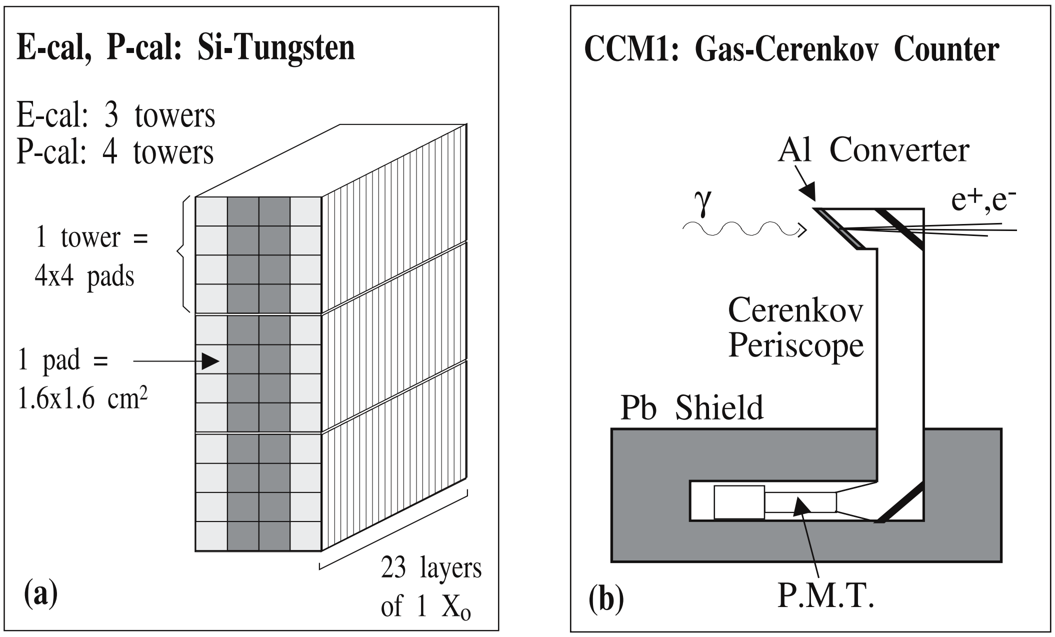

Figure 5: (a) The Silicon-Tungsten calorimeters ECAL and PCAL. (b) The gas Čerenkov monitor CCM1; monitors EC31 and EC37 are of similar construction.

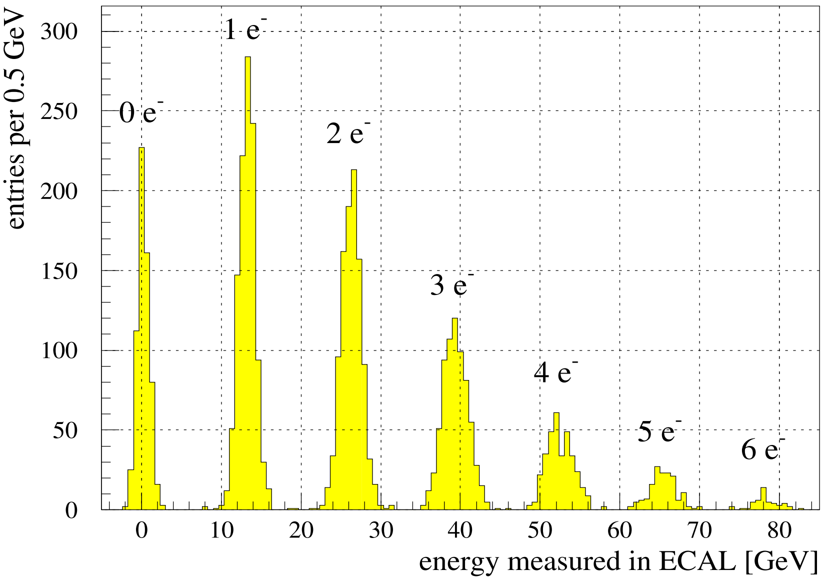

Figure 6: Energy measured by the calorimeter ECAL during a calibration run with 13 GeV electrons.

the electron beam where they could be detected in a similar calorimeter (PCAL). High-energy backscattered photons were detected by monitor CCM1 (Fig 5b) which observed Čerenkov light from the conversion of the photons in 0.2 radiation lengths of aluminum. Scattered electrons in the range 30-40 GeV were detected in Čerenkov monitors EC31 and EC37 of similar construction.

The Silicon-Tungsten calorimeters are segmented vertically and horizontally in 12 rows and 4 columns of 1.6 cm $\times$ 1.6 cm pads and in four longitudinal groups of 23 radiation lengths total thickness. The calorimeter energy resolution is $\sigma_E/E \approx 0.25/\sqrt{E(\mathrm{GeV})}$, whereas the size of the pads resulted in a momentum resolution of $\sigma_p/p \approx 0.04$. Both ECAL and PCAL were calibrated in parasitic running of the FFTB to the SLC program in which linac-halo electrons of energies between 5 and 25 GeV were transmitted by the FFTB when tuned to a lower energy. The number of such electrons varied between 1 and 100 per pulse, which provided an excellent calibration of the ECAL and PCAL over a wide dynamic range. Figure 6 shows the ECAL response to a 13 GeV test beam. The peaks corresponding to events with 0 to 6 electrons per beam bunch can easily be distinguished. The calibration runs also allowed a check of the field maps of the FFTB dump magnets that are used in our spectrometer.

2.2 Phase II and III

The setup of future phases of the experiment are sketched in Fig. 7 and Fig. 8. In the second phase a thin foil or wire will convert high-energy Compton photons to pairs that will be analyzed in a pair spectrometer based on CCD's. The CCD pair spectrometer, sketched in Fig. 9, will reconstruct the photon-energy spectrum with resolution sufficient to discern the effective mass $\overline{m}$.

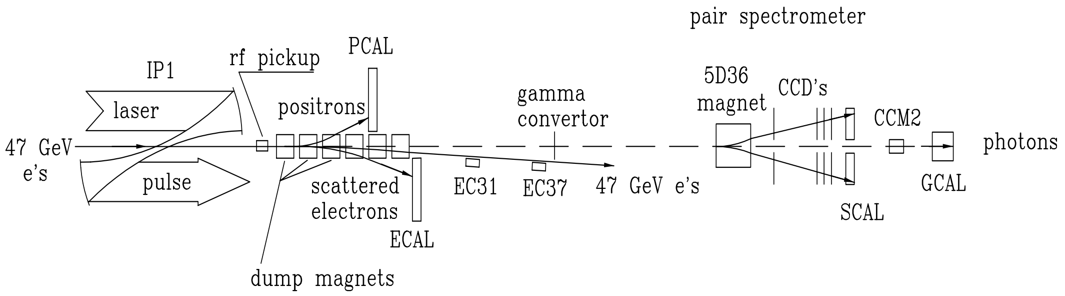

Figure 7: Sketch of the experiment with the addition of a pair spectrometer to analyze converted Compton photons.

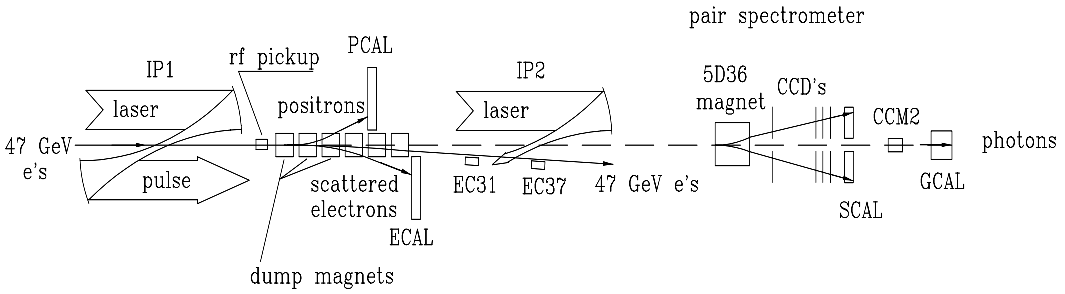

Figure 8: Sketch of the experiment with the addition of a second laser interaction point to study pair creation by light.

In a third phase (Fig. 8), part of the laser beam will collide with the high-energy Compton photons at a new interaction point, IP2, and the invariant mass of resulting pairs will be analyzed in the pair spectrometer free from backgrounds of electrons and positrons produced at IP1.

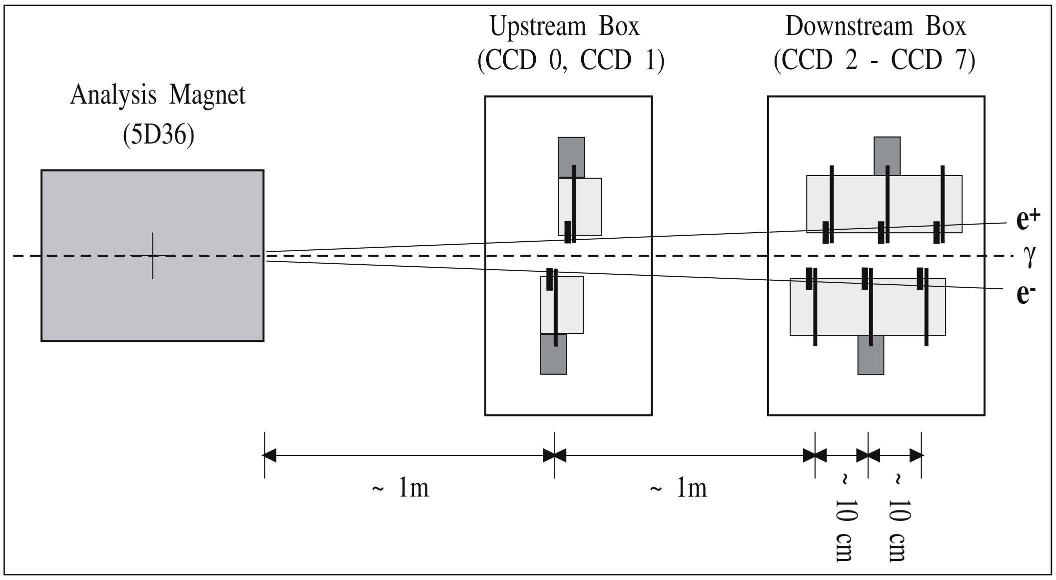

Figure 9: The CCD pair spectrometer.

3 The Laser System

The beam from a chirped-pulse-amplified terawatt Nd:glass laser system[24,25] is focused by off-axis-parabolic mirrors of 30 cm focal length with a 17° crossing angle onto the electron beam at IP1. The laser system is shown in Fig. 10 and delivered 1.5-ps (fwhm) wide pulses at 0.5 Hz of up to 1.2 J of infrared light, or 1 J of green light after frequency doubling in a KDP crystal. The relatively high repetition rate is achieved in a final laser amplifier with slab geometry.[26]

The laser-oscillator mode locker is synchronized to the 476-MHz drive of the SLAC linac klystrons via a rf/optical feedback system.[27] The observed jitter between the laser and linac pulses was 2 ps (rms).[28] The laser-pulse energy and area were measured for each shot. The laser pulse length was available for each shot during infrared running and as averages over short time intervals for green.

The peak focused laser intensity was obtained for infrared pulses of energy U = 800 mJ, focal area A = 60 μm^2 and pulse width Δt = 1.5 ps, for which $I = U/A\Delta t \approx 10^{18}$ W/cm^2 at $\lambda = 1054$nm, corresponding to a value of $\eta = 0.6$. Electrons that passed through the focus of the laser at peak intensity had a 25% probability of interacting.

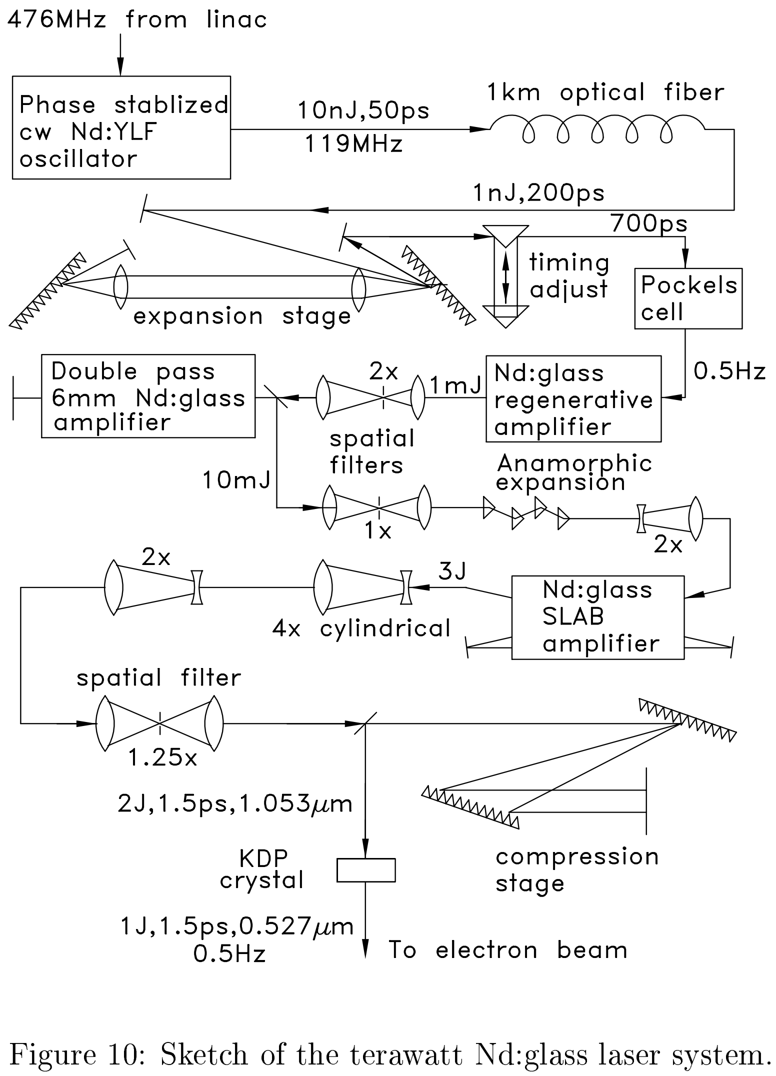

Figure 10: Sketch of the terawatt Nd:glass laser system.

4 Laser Pulse and Electron Bunch Overlap

The electron beam was operated at 10-30 Hz with an energy of 46.6 GeV and emittances $\varepsilon_x = 3 \times 10^{-10}$ m-rad and $\varepsilon_y = 3 \times 10^{-11}$ m-rad. The beam was tuned to a focus with $\sigma_x = 60$ μm and $\sigma_y = 70$ μm at the laser-electron interaction point. The electron bunch length was expanded to 3.6 ps (rms) to minimize the effect of the time jitter between the laser and electron pulses. Typical bunches contained 5×10^9 electrons. However, since the electron beam was significantly larger than the laser focal area only a small fraction of the electrons crossed through the peak field region.

The spatial and temporal overlap of the electron and laser beams was monitored by observing the Compton scattering rate in the ECAL and CCM1 detectors during horizontal (x), vertical (y) and time (t) scans of one beam across the other. Figure 11 shows results of a combined x-t scan. Figure 11a is derived from scattered photons and is dominated by ordinary Compton scattering. The slope of the data agrees with the 17° beam-crossing angle. Figure 11b is derived from electrons of energy less than 25.6 GeV where single Compton scattering does not contribute. The peak in Fig. 11b has a smaller space-time extent than that in Fig. 11a because the nonlinear process is more probable in the higher intensity regions of the laser beam.

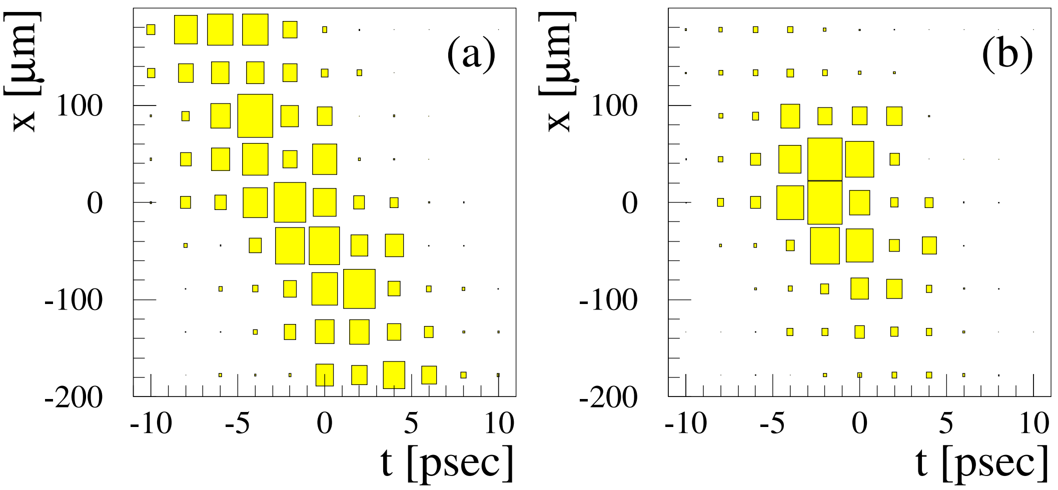

Figure 11: Observed rates of (a) ordinary and (b) nonlinear and multiple Compton scattering as a function of x and t offsets between the electron and laser beams. The area of each box is proportional to the signal size.

5 First Results

5.1 Electron Beam Polarization Measurement

In the commissioning of the present experiment in April 1994 a measurement was made of the longitudinal polarization of the electron beam. For this measurement, data were collected with circularly polarized green laser pulses of ~ 3 mJ energy and ~ 50 ps pulse width. To minimize the effect of shower spreading in the calorimeter, only the signal from the second longitudinal layer of ECAL (out of 23 layers) was used as a measure of the number of incident electrons.

The top row of ECAL was centered at $E = 25.6$ GeV, the electron energy corresponding to the zero crossing of the Compton asymmetry

$$A(E) \equiv \frac{N_+(E) - N_-(E)}{N_+(E) + N_-(E)}$$

where $N_+(E)$, $N_-(E)$ refer to the signal in layer 2 of ECAL for events with electron polarization along/against the momentum vector.

Figure 12 shows that the measured Compton asymmetries in the top 4 ECAL rows are in good agreement for the two data sets taken with the right and left circularly polarized laser.

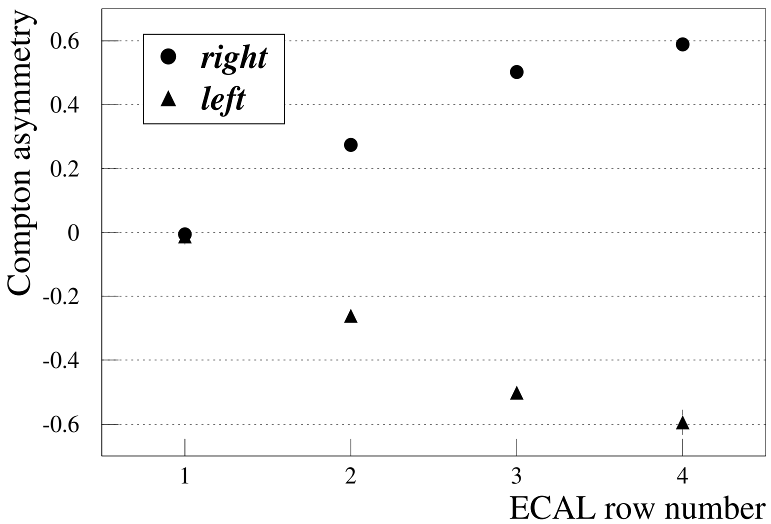

Figure 12: Measured Compton asymmetry in top 4 ECAL rows for right and left circularly polarized laser beams.

A fit of the observed asymmetries gave the result $P_e = 0.81^{+0.04}_{-0.01}$ for the longitudinal polarization of the electron beam,[30] in good agreement with measurements of the SLD collaboration. The upper error of 0.04 on the polarization is due to the uncertainty in the degree of circular polarization of the laser, and could readily be reduced to 0.01 in any future measurements.

5.2 Nonlinear Compton Scattering

Nonlinear effects in Compton scattering were investigated by detecting the scattered electrons. The ECAL sampled the scattered electrons in energy intervals about 1.5 GeV wide. The highest energy sampled was 30 GeV, but the maximum sampled energy could be reduced by lowering the entire calorimeter away from the beam. When positioned with maximum energy below 25.6 GeV, only electrons from nonlinear scattering were detected.

An ECAL channel saturated at 12 TeV, while at peak laser intensity some 10^7 Compton scatters occur per pulse. Hence the ECAL could not be used to study ordinary Compton scattering for laser intensities higher than about 0.001 of peak. Shower cross-talk between calorimeter pads and backsplash from ordinary Compton-scattered electrons that hit components of the beamline limited the dynamic range of ECAL to about 100:1. Because of this and the rapidly decreasing electron yield at lower energies only data from the top 4 calorimeter rows were used in the analysis. Thus the complete mapping of the nonlinear Compton spectrum required data collection at several laser intensities and positions of the ECAL. Figure 13 summarizes the data collection strategy for runs with the infrared laser beam. The accessible range of the scattered electron energy versus the laser intensity is shown as the white area. In the dark shaded area some of the ECAL channels would saturate, while the light shaded area corresponds to signals in ECAL pads dominated by cross-talk and background.

Data were collected with circularly polarized beams at laser pulse energies between 14 and 800 mJ at $\lambda_0 = 1054$ nm, and between 7 and 320 mJ at 527 nm. The energy measured in the calorimeter pads, each of which accepted a limited momentum bite, gave the spectrum of electrons scattered in that pulse. Corrections were applied for shower cross-talk between calorimeter pads, and for backgrounds from high energy Compton scattered electrons that hit beamline components. Two methods were used to estimate the corrections, based on shower spread in-

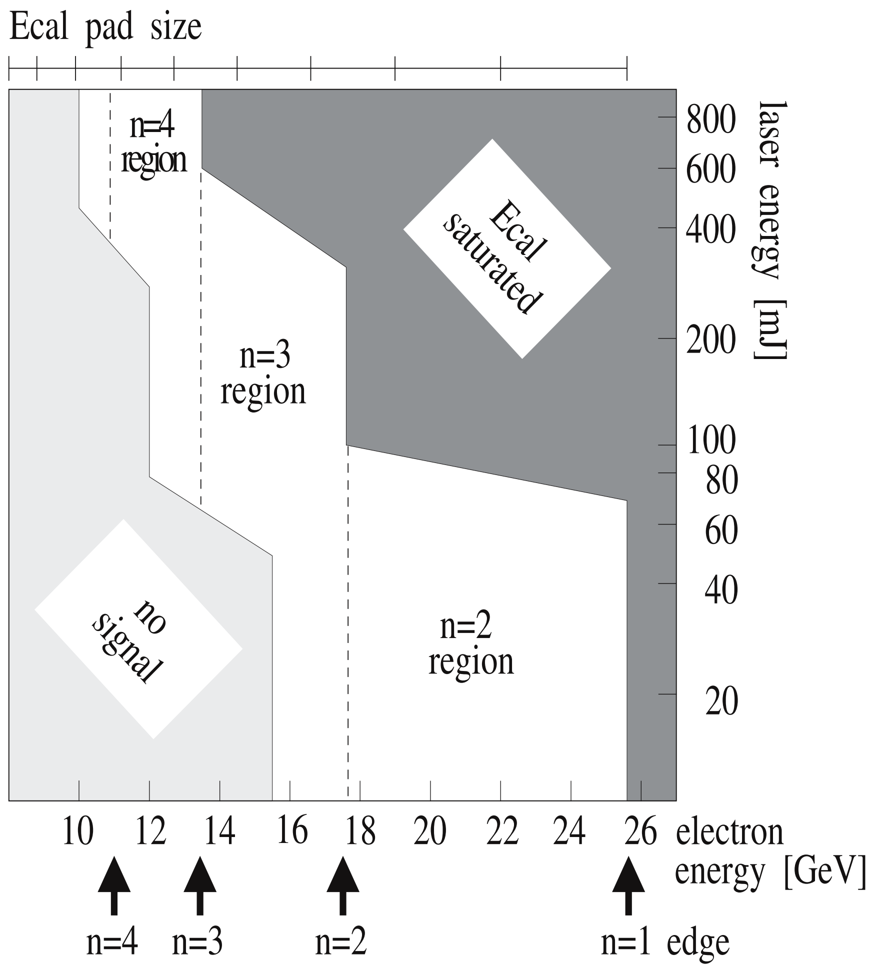

Figure 13: Data collection strategy for the infrared laser beam. The size of an ECAL pad is shown at the top of the figure. The minimum energy of an electron scattered off n laser photons is indicated at the bottom.

formation from calibration runs and on signal in calorimeter channels outside the acceptance for Compton scattering. The average of the two methods is used, and the difference is taken as a contribution to the systematic uncertainty.

Because of the time jitter between the electron and laser pulses the interaction flux was not readily determined from beam measurements alone. Instead, we use the rate of Compton-scattered photons, N_γ, measured by CCM1 as a normalization. To first order the normalized rate equals the normalized cross section:

$$\frac{1}{N_\gamma}\frac{dN}{dE} \approx \frac{1}{\sigma}\frac{d\sigma}{dE},$$

where σ is the total cross section which is close to the ordinary Compton cross section, $\sigma_C = 1.9 \times 10^{-25}$ cm^2 for infrared and 3.0×10^{-25} cm^2 for green.

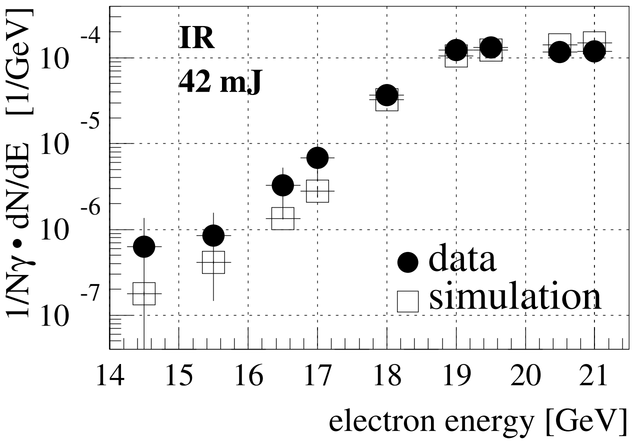

Figure 14: Energy spectra of scattered electrons as observed in the ECAL calorimeter for infrared laser pulses of 42 mJ energy.

In Fig. 14, the rate of scattered electrons normalized to the Compton γ-ray rate is plotted against the electron energy, for infrared laser pulses with a nominal energy of 42 mJ. The open squares represent a simulation of each pulse using the corresponding laser and electron beam parameters at the collision point. The simulation includes both nonlinear and multiple ordinary Compton scatterings. Only energies below the minimum for single Compton scattering are shown. The plateau at 19-21 GeV corresponds to two-photon scatters, and the fall-off at 17-18 GeV is evidence for the two-photon kinematic limit at 17.6 GeV as smeared by the spatial resolution of the calorimeter.

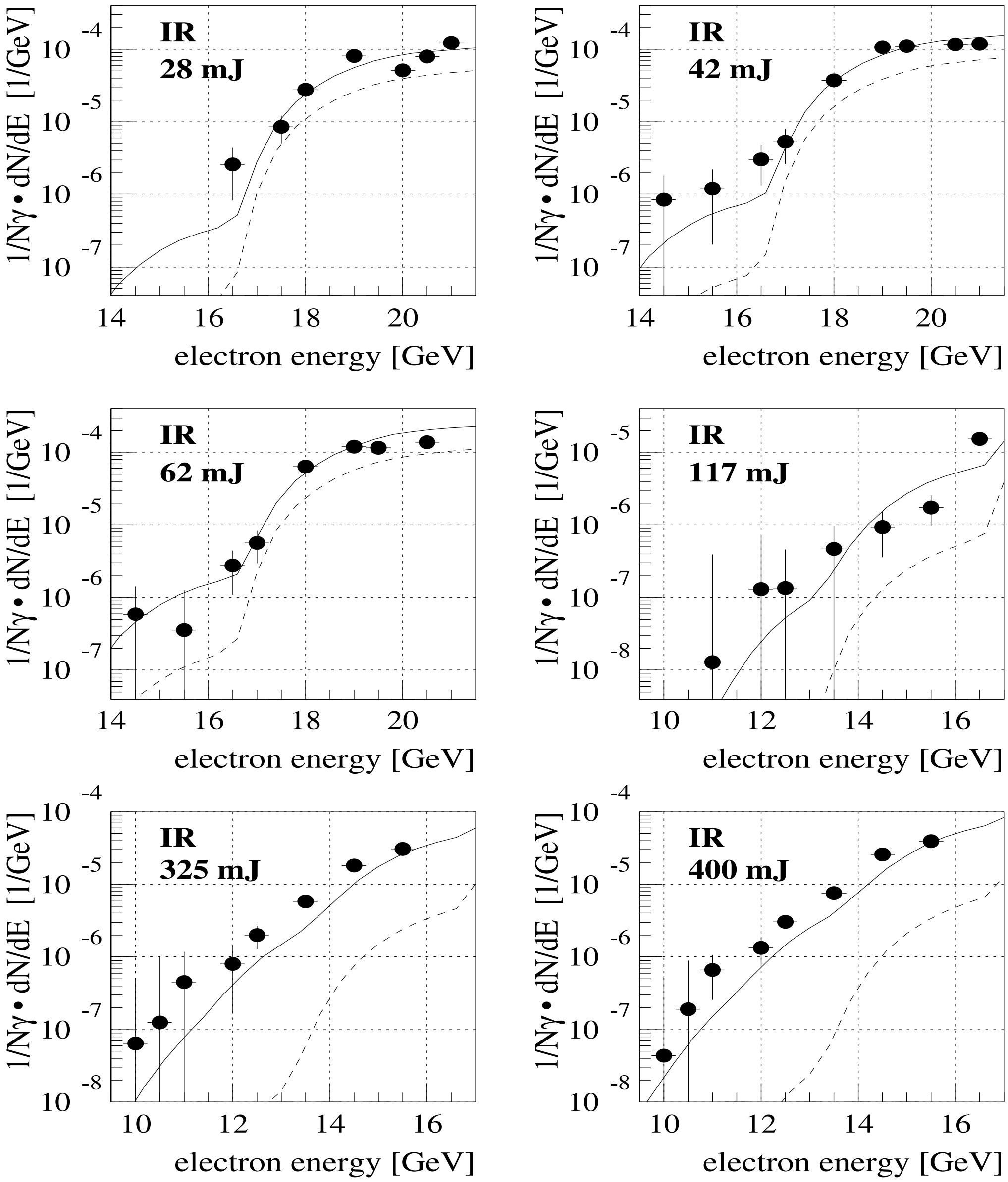

Figure 15: Energy spectra of scattered electrons for infrared laser pulses with circular polarization and nominal energies between 28 mJ and 400 mJ. The data (filled-in circles) has been scaled to standard values of the interaction geometry. The solid line represents the simulation and the dashed line shows the simulated contribution for multiple ordinary Compton scattering only.

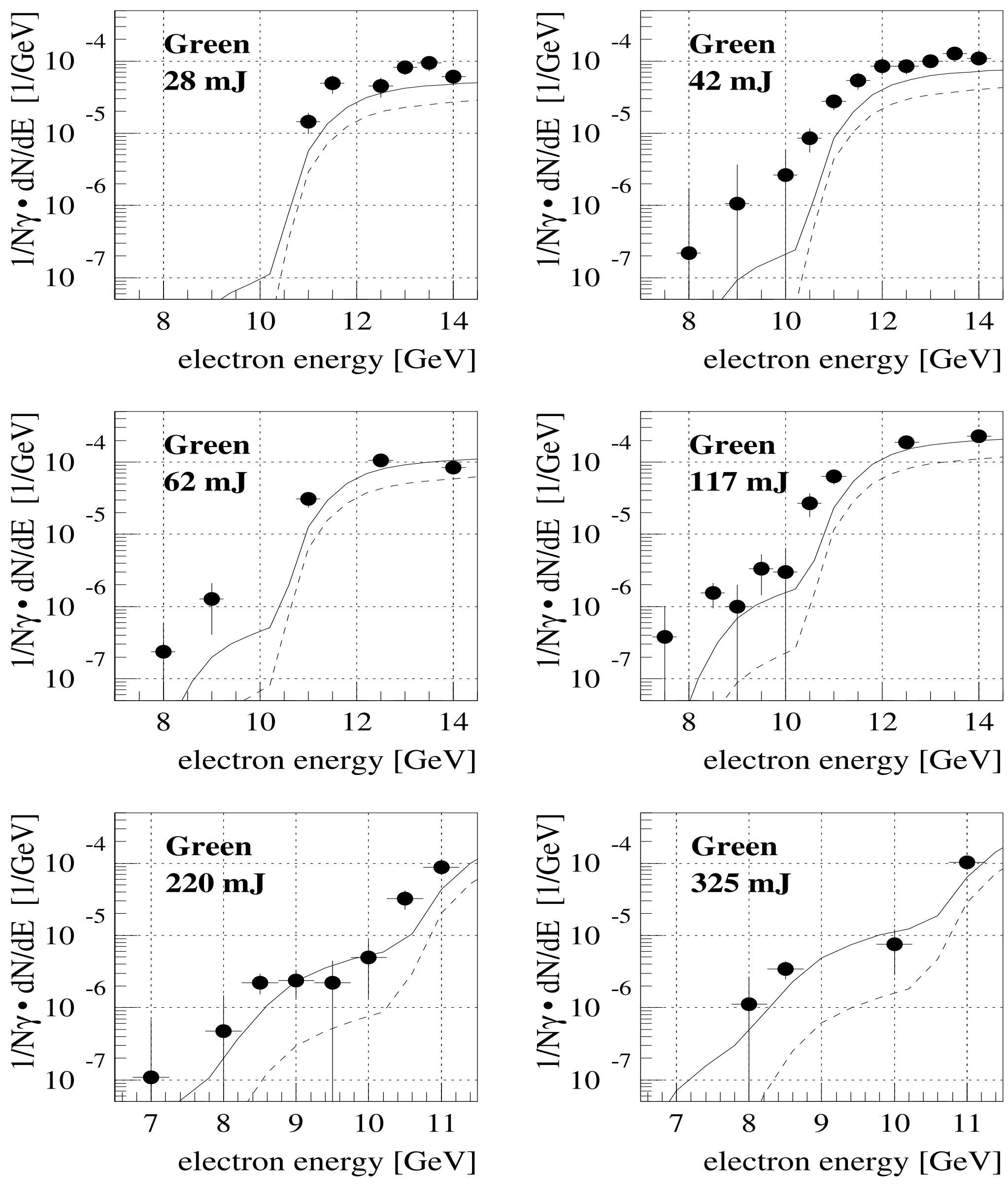

Figure 16: Energy spectra of scattered electrons for green laser pulses with circular polarization and nominal energies between 28 mJ and 325 mJ. The data (filled-in circles) has been scaled to standard values of the interaction geometry. The solid line represents the full simulation and the dashed line shows the simulated contribution for multiple ordinary Compton scattering only.

To compensate for small variations in the beam parameters during the run, the data in Figs. 15-17 have been scaled by the ratio of the simulated rates at observed and standard values of electron and laser beam-spot dimensions. Figure 15 shows results from infrared data at 6 laser energies differing by more than an order of magnitude. The full simulation is shown as the solid curve. The rate calculated for multiple ordinary Compton scattering is shown as the dashed curve which clearly cannot account for the observations. The kinematic limit for $n = 3$ scattering at 13.5 GeV cannot be resolved in the data, but the expected effect is only a very small shoulder in the rate. The two last plots at laser pulse energies of 325 and 400 mJ show proof of $n = 4$ scattering in the momentum range of 11-13 GeV. Figure 16 shows similar results for green data at 6 laser energies between 28 and 325 mJ. The $n = 2$ plateau at 12-14 GeV as well as the $n = 2$ kinematic limit at 10.9 GeV can be discerned in the data. The data points between 8 GeV and 10 GeV in the plots with the highest laser intensities are evidence of $n = 3$ scattering in green data.

In Fig. 17 we illustrate the rise in the normalized nonlinear rate with laser intensity. As the rates are normalized to the total Compton-scattering photon signal which is primarily ordinary Compton scattering, data at electron energies dominated by order n should vary with laser pulse intensity as I^{n-1}. The shaded bands shown for each electron momentum represent the simulation including an uncertainty in laser intensity of $\Delta I/I = 0.3$ for infrared and $\Delta I/I =^{+0.5}_{-0.3}$ for green laser pulses. The $n = 2$ and $n = 3$ data sets in Fig. 17a and the $n = 2$ set in Fig. 17b agree reasonably well with expectations for the slopes as well as the magnitudes of the rates. For the lowest electron momenta shown in Figs. 17a and 17b, only the data at the highest laser intensities represents a signal well above background and therefore the observed slope does not agree well with expectations.

The error bars shown in Fig. 14 represent statistical uncertainty in the number of scattered electrons and the systematic uncertainty in the correction for backgrounds in the calorimeter. In Figs. 15-17 the error bars also include uncertainties in the scaling to standard beam conditions.

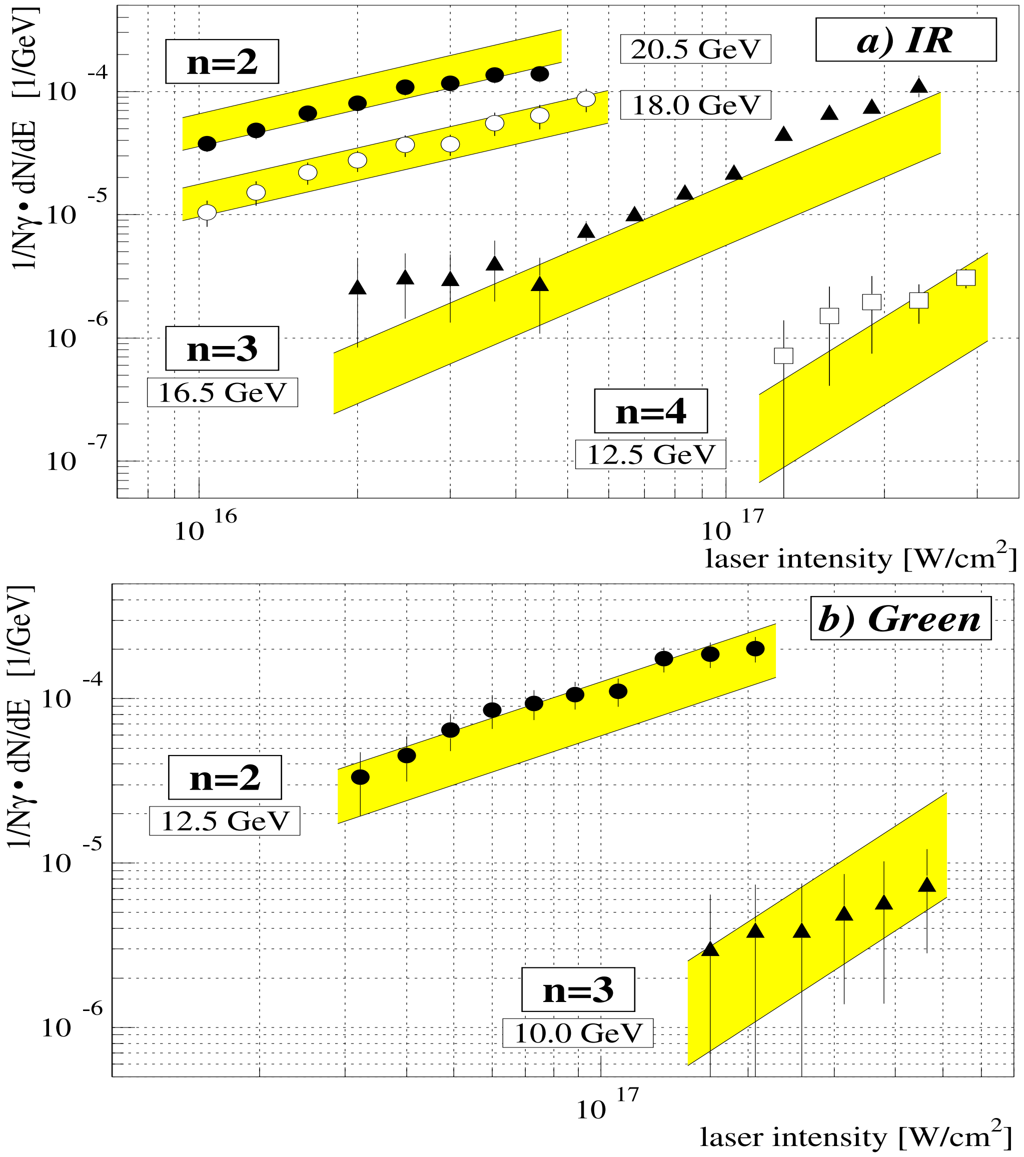

Figure 17: The normalized rate of scattered electrons of energies corresponding to n = 2, 3 and 4 laser photons per interaction versus the intensity of the laser field at the interaction point for (a) infrared and (b) green laser pulses. The bands represent a simulation of the experiment including an uncertainty in laser intensity of $\Delta I/I = 0.3$ for infrared and $\Delta I/I =^{+0.5}_{-0.3}$ for green.

6 Conclusion

We measured the longitudinal polarization of the electron beam at the FFTB and found good agreement with measurements of the SLD collaboration.

We observed at two different laser wavelengths a clear signal for nonlinear Compton scattering in the spectrum of the scattered electrons. At the highest laser intensities achieved, up to 4 laser photons were absorbed in a single scattering event. The dependence of the scattered electron rate on electron momentum and laser intensity agree within experimental uncertainty with theory[10] over a wide range of laser pulse energies.

References

[1] G.A. Schott, *Electromagnetic Radiation*, (Cambridge University Press, 1912).

[2] T.J. Englert and E.A. Rinehart, Phys. Rev. A **28**, 1539 (1983).

[3] See, for example, M. Billardon *et al.*, J. de Phys., Colloq. **44**, C1 (1983).

[4] D.M. Volkov, Z. Phys. **94**, 250 (1935).

[5] See also V.B. Berestetskii *et al.*, *Quantum Electrodynamics*, 2nd ed., (Pergamon Press, 1982), §40.

[6] N.D. Sengupta, Bull. Math. Soc. (Calcutta) **44**, 175 (1952).

[7] L.S. Brown and T.W.B. Kibble, Phys. Rev. **133**, A705 (1964).

[8] A.I. Nikishov and V.I. Ritus, Sov. Phys. JETP **19**, 529, 1191 (1964); **20**, 757 (1965); see also §101 of ref.[5]

[9] I.I. Gol'dman, Sov. Phys. JETP **19**, 954 (1964); Phys. Lett. **8**, 103 (1964).

[10] N.B. Narozhny *et al.*, Sov. Phys. JETP **20**, 622 (1965).

[11] T.W.B. Kibble, Phys. Rev. Lett. **16**, 1054 (1966); Phys. Rev. **150**,1060 (1966).

[12] J.H. Eberly and A. Sleeper, Phys. Rev. **176**, 1570 (1968).

[13] C.I. Moore *et al.*, Phys. Rev. Lett **74**, 2439 (1995).

[14] F. Sauter, Z. Phys. **69**, 742 (1931). See also §129, prob. 2 of ref.[5]

[15] O. Klein, Z. Phys. **53**, 157 (1929).

[16] W. Heisenberg and H. Euler, Z. Phys. **98**, 718 (1936).

[17] G. Breit and J.A. Wheeler, Phys. Rev. **46**, 1087 (1934).

[18] H.R. Reiss, J. Math. Phys. **3**, 59 (1962). Phys. Rev. Lett. **26**, 1072 (1971).

[19] M. Bell and J.S. Bell, Part. Acc. **24**, 1 (1988); R. Blankenbecler and S.D. Drell, Phys. Rev. Lett. **61**, 2324 (1988); M. Jacob and T.T. Wu, Nucl. Phys. **B303**, 373, 389 (1989); **B327**, 285 (1989); P. Chen and K. Yokoya, Phys. Rev. Lett. **61**, 1101 (1988); V.N. Baier *et al.*, Nucl. Phys. **B328**, 387 (1989); P. Chen and V.L. Telnov, Phys. Rev. Lett. **63**, 1796 (1989); R. Blankenbecler *et al.*, Phys. Rev. D **40**, 2462 (1989).

[20] I.F. Ginzburg *et al.*, Nucl. Instr. and Meth. **205**, 47 (1983).

[21] K.O. Mikaelian, Phys. Rev. D **17**, 750 (1978); **30**, 1115 (1984); I.F. Ginzburg *et al.*, Nucl. Phys. **B228**, 285 (1983).

[22] P. Chen and R.B. Palmer, SLAC-PUB-5966 (Nov. 1992).

[23] V. Balakin *et al.*, Phys. Rev. Lett. **74**, 2479, (1995).

[24] D. Strickland and G. Mourou, Opt. Comm. **55**, 447 (1985).

[25] C. Bamber *et al.*, U. Rochester preprint UR-1428 (June 1995).

[26] W.S. Martin and J.P. Chernoch, U.S. Patent 3633126 (1972).

[27] M.J.W. Rodwell *et al.*, Opt. Lett. **11**, 638 (1986).

[28] T. Kotseroglou *et al.*, U. of Rochester preprint UR-xxxx, in preparation.

[29] S.C. Berridge *et al.*, IEEE Trans. Nucl. Sci. **37**, 1191 (1990).

[30] M.B. Woods *et al.*, E144 Internal Note (Oct. 17, 1994).